Journal of the European Ceramic Society xxx (xxxx) xxx–xxx

Contents lists available at ScienceDirect

Journal of the European Ceramic Society

journal homepage: www.elsevier.com/locate/jeurceramsoc

Feature article

High temperature creep of 20 vol%. SiC-HfB_2 UHTCs up to 2000 °C and the effect of La_2O_3 addition

E. Zapata-Solvas[a,b,*], D. Gómez-García[a,c], A. Domínguez-Rodríguez[c], W.E. Lee[b]

[a] Instituto de Ciencia de Materiales de Sevilla, CSIC-Universidad de Sevilla, 41092 Sevilla, Spain
[b] Centre for Nuclear Engineering & Dpt. of Materials, Imperial College London, SW7 2AZ, UK
[c] Dpto. Física de la Materia Condensada, Universidad de Sevilla, 41012 Sevilla, Spain

ARTICLE INFO

Keywords:
Ultra-high temperature ceramics
Creep
Cavitation damage
Reaction damage
Limited ductility

ABSTRACT

High temperature compressive creep of SiC-HfB_2 UHTCs up to 2000 °C has been studied. Microstructural analysis after deformation reveals formation of new phases in the Hf-B-Si and Hf-B-Si-C systems, which are responsible for the poor creep resistance. RE oxide additions have a negative effect reducing the creep resistance of SiC-HfB_2 UHTCs. A simplistic analysis for the required creep resistance is described, indicating that only SiC-HfB_2 UHTCs could withstand re-entry conditions for 5 min in a single use. However, RE oxide addition to SiC-HfB_2 UHTCs does not provide the required creep resistance for them to be candidate materials for hypersonic applications.

1. Introduction

Me borides and carbides (Me = Zr or Hf) with melting points in excess of 3000 °C are promising candidates for thermal protection systems (TPS) in hypersonic vehicles, including sharp-leading edges (SLE) and sharp-nose cones (SNC) [1,2], and belong to a family of materials termed ultra-high temperature ceramics (UHTCs). Ideally, UHTCs components for hypersonic applications have to maintain a stable structure under the operating conditions, which involve no phase transformations and no shape changes during operating conditions. No shape changes require high creep resistance and, e.g the components should deform no further than the elastic limit to be reusable. In addition, UHTCs components require a combination of properties at high temperatures, such as high temperature strength, oxidation resistance, with high thermal conductivity being particularly desirable to maximize thermal transport during exposure in high-temperature reactive environments [3]. Me borides possess a better combination of oxidation resistance and thermal conductivity than Me carbides and have been the subject of intense research over the last 15 years [4,5]. Moreover, ZrB_2 and HfB_2 exhibit higher thermal conductivity (~100 W/(m K)) at room temperature (and > 50 W/(m K) at 1900 °C) [6] than their respective carbides (< 40 W/(m K) from room temperature to 800 °C) [5]. However, the oxidation resistance of MeB_2 is relatively poor which could compromise the structural stability of UHTCs components under hypersonic operating conditions. As a consequence, UHTCs research has focused over the last decade on the oxidation resistance of MeB_2-based UHTCs and different approaches to improve oxidation resistance have been attempted; (i) Adding different Si-containing compounds to incorporate different elements in the outer protective borosilicate (BS) coating, which results in an increase of viscosity and melting temperature as well as a reduction in the oxygen diffusion coefficient through the BS [7]; (ii) Adding different diborides, such as TaB_2, TiB_2 or CrB_2, as BS glasses containing oxides of the elements listed are immiscible leading to phase separation, increasing their viscosity and melting temperature [8]; (iii) Adding rare earth compounds that could lead to a protective refractory coating formed during the oxidation of the UHTCs components [9,10]; (iv) Adding low contents of rare earth compounds (< 3 vol%), such as La_2O_3, which lead to the formation of MeO_xC_y particles in the oxide scale as a result of increasing viscosity of BS, leading to a long-term stabilization of the oxide scale [11].

The composition that has received most attention to date and is currently considered as a baseline UHTCs composition for hypersonic TPS development is SiC-reinforced UHTCs, with a SiC content ranging from 10 to 30 vol.% [2,9]. Oxidation of SiC produces an outer BS protective glass that could protect UHTCs components up to ~1650 °C, at which temperature pure SiO_2 melts and bulk UHTCs would be exposed to continuous oxidation. Although the BS coating melts at lower temperatures it could withstand temperatures up to 2000 °C for up to 1 h under static oxidation conditions [12–17]. However, this liquid layer will be blown away during a hypersonic reentry.

On the other hand, hypersonic applications require high strength at high temperature and estimated conditions for hypersonic re-entry are ~1800 °C and ~400 MPa [3]. Furthermore, the latter conditions are at the less harsh end of reentry conditions and in the long term, the

* Corresponding author at: Centre for Nuclear Engineering & Dpt. Of Materials, Imperial College London, SW7 2AZ, UK.
E-mail address: eugenio.zapata-solvas@imperial.ac.uk (E. Zapata-Solvas).

http://dx.doi.org/10.1016/j.jeurceramsoc.2017.08.028
Received 27 April 2017; Received in revised form 16 August 2017; Accepted 19 August 2017

development of UHTCs able to withstand temperatures in excess of 2000 °C under the same stresses will be required. This requirement has led the scientific community to develop high strength UHTCs components, as high as 1 GPa at room temperature (RT) [18,19]. Moreover, SiC reinforced MeB_2 have shown the highest RT strength values [20]. However, UHTCs must withstand extreme conditions of temperature and stress under harsh environments and the available data about high temperature mechanical properties, i.e. strength and creep resistance, is scarce. Concerning HT strength measurements, there have been few reports of the strength of UHTCs at the expected operating temperatures. ZrB_2 shows a strength value of ~220 MPa in the temperature range from 1600 °C to 2200 °C [21]. Hu and Wang reported a strength of ~220 MPa for ZrB_2-30 vol.% SiC at 1800 °C [22] while Neuman et al. found a strength of 540 MPa at 1800 °C and 260 MPa at 2200 °C in ZrB_2-30 vol.% SiC + 2 wt.% B_4C illustrating the impact on strength of a small amount of B_4C [23]. Highest strength at high temperature till date, 290 MPa at 2200 °C and 2300 °C, was reported by Neuman et al. in ZrB_2-10 vol.% ZrC [24]. However, the strength of ZrB_2-10 vol.% ZrC at 1800 °C was 345 MPa which is lower than the 540 MPa of ZrB_2-30 vol.% SiC + 2 wt.% B_4C at 1800 °C. All the strengths mentioned above were measured in inert atmosphere. However, measured strengths in air for ZrB_2-30 vol.% SiC + 2 wt.% B_4C were ~360 MPa at 1500 and 1600 °C [25], much lower than the 540 MPa shown at 1800 °C in Ar [23]. The main limitation for high temperature mechanical properties testing at 2000 °C is that the majority of commercial furnaces are limited to 1600 °C, especially those furnaces able to test in air, and there are few facilities around the world with the capability of testing at 2000 °C under inert atmospheres. Those strengths are below the expected stress conditions mentioned above, which have been predicted considering elastic deformation of UHTCs components. Therefore, the study of active deformation mechanisms, which could produce a stress relaxation during hypersonic re-entry to avoid mechanical failure of UHTCs, becomes crucial. Furthermore, the structure of hypersonic vehicles depends on the structural integrity of the UHTCs components, which is directly related to their creep resistance. High creep resistance is desirable to avoid shape changes during plastic deformation. For example, the edge of SLEs and SNCs are the areas of UHTCs components exposed to highest temperature and maximum stresses, which are susceptible to plastic deformation under the operating conditions. Therefore, a small change in the radius of curvature of SLE or SNC during hypersonic re-entry could have a significant negative impact on maneuverability and subsequent vehicle aerodynamics.

Few creep studies have been carried out on UHTCs, with most that have being for SiC-reinforced UHTCs. All have been performed in flexure [22–26] and for deformations < 1% [26–29]. Deformation in flexure exceeding 2% leading to mechanical failure in 20 vol.% SiC-reinforced ZrB_2 [28], has been examined by Guo et al., who observed formation of isolated cavities in the tensile side of 30 vol.% SiC-reinforced ZrB_2, nucleated always on SiC particle boundaries [28] for deformations as low as 0.2% at 1500 °C under strain rates of $\sim 2 \times 10^{-9}\,s^{-1}$. Talmy et al. observed crack formation during the tertiary stage of creep in the tensile side of 50 vol.% SiC-reinforced ZrB_2, presumably related to cavity nucleation, and determined that the controlling deformation mechanism is SiC grain boundary sliding [27]. Bird et al. reported formation of cavities in 20 vol.% SiC-reinforced ZrB_2 above 1600 °C and suggested that cavitation partially accommodates grain boundary sliding [29]. In addition, it was determined that diffusional creep accommodated by lattice diffusion is the active deformation mechanism below 1600 °C and grain boundary sliding above 1600 °C [29]. Note that true creep behavior is related to flexural creep in the case of symmetric creep, i.e. in which the tensile creep rate is the same as that in compression. Gangireddy et al. suggested that 30 vol.% SiC-reinforced ZrB_2 has symmetric creep for strains below 1% [26] based on transmission electron microscopy (TEM) observation of the absence of glassy films at grain boundaries in 10 vol.% SiC-reinforced ZrB_2 fabricated by the same hot press (HP) method, carried out by Jayaseelan et al. [30]. However, Bird et al. quantified a neutral axis shift during deformation in 20 vol.% SiC-reinforced ZrB_2 which confirms the existence of asymmetric creep [31]. The asymmetry between tensile and compressive creep is a typical feature of SiC-, Al_2O_3- or Si_3N_4-based ceramics, in which an easily deformable glass is present at the grain boundaries showing an accelerated creep under tension [32,33]. In addition, the presence of cavitation during plastic deformation as observed in reaction bonded SiC is evidence of asymmetric creep behavior [33]. Cavitation usually leads to asymmetric creep behavior as coalescence of cavities is easier under tensile than compressive creep [34]. Monolithic ceramics, such as Y-TZP and Al_2O_3, show symmetric creep behavior [32,35].

Cavitation in tensile or flexure creep makes the assessment of active deformation mechanisms more difficult as deformation mechanisms are usually the combination of at least two deformation mechanisms [33,34]. Therefore, deformation mechanisms are usually studied in compression by the ceramics community [36,37] unless the stresses are low enough to have pure diffusional creep without cavitation [34]. Moreover, the symmetric creep behavior of SiC-reinforced ZrB_2 ceramics is questionable as there are no data under tensile or compressive creep and the presence of cavities after deformation has been detected only on the tensile side. The work described in this paper is the first to examine compressive creep of 20 vol.% SiC-HfB_2 ceramics in an attempt to identify the active deformation mechanisms from 1800 °C–2000 °C, which is the expected temperature range for SiC-reinforced MeB_2 UHTCs under hypersonic regimes. Compressive creep is analyzed in terms of a constitutive creep equation [37];

$$\dot{\varepsilon} = A\frac{Gb}{kT}\left(\frac{b}{d}\right)^{p}\left(\frac{\sigma}{G}\right)^{n} D_0 exp\left(-\frac{Q}{kT}\right) \quad (1)$$

where $\dot{\varepsilon}$ is the strain rate, A dimensionless constant, G the shear modulus, b the magnitude of the Burgers vector or any characteristic length scale in the material, k the Boltzmanńs constant, T the absolute temperature, d the average grain size and σ the applied stress. The term D_0 is the frequency factor of an appropriate diffusion coefficient responsible for the migrating species involved in the accommodation process. Q is the activation energy of the active diffusion phenomena. A deformation mechanism is usually identified by the determination of p, n, Q and through the observation of microstructure after deformation.

Recently, it was reported that the addition of 2 wt.% La_2O_3 to SiC-reinforced MeB_2 was beneficial for long-term oxidation processes as the oxide layer showed better stability than SiC-reinforced MeB_2 due to MeO_xC_y formation within the oxide layer [38]. Therefore, the aim of this study is to characterize the structural properties and plastic response of 20 vol.% SiC-reinforced HfB_2 and 2 wt.% La_2O_3 + 20 vol.% SiC-reinforced HfB_2 under compression from 1800 °C to 2000 °C and determine whether SiC-reinforced HfB_2 UHTCs are structurally stable under such conditions.

2. Experimental procedure

HfB_2 powder (> 99%, d_{50} ~ 5.0 μm, ρ = 10.5 g/cm^3, Sigma Aldrich, Gillingham, UK), SiC powder (α-SiC, 99%, d_{50} ~ 0.7 μm, ρ = 3.217 g/cm^3, Good Fellow Chemicals, Huntingdon, UK) and La_2O_3 (> 99%, d_{50} ~ 10 μm, ρ = 6.51 g/cm^3, Fluka chemicals supplied through Sigma Aldrich, Steinheim, Germany) were used to form different UHTC compositions; HfB_2 + 20 vol.% SiC (HS20) and HfB_2 + 20 vol.% SiC + 2 wt.% La_2O_3 (HS20La). Ceramic powders were processed and then sintered using Spark Plasma Sintering (SPS) as described previously [10]. The main microstructural features of SPS UHTCs [11,19] are; (I) high density (> 99% of theoretical relative density); (II) HfB_2-based UHTCs contain an inhomogeneous dispersion of SiC throughout the HfB_2 matrix with SiC agglomerates as large as 20 μm; and (III) La_2O_3 particles are often in close proximity to SiC particles and improve the SiC dispersion throughout the HfB_2 matrix.

SPS (40 mm dia × 5 mm thick) billets were cut using electro-

discharge machining (EDM) to obtain 2.5 mm × 2.5 mm × 4.5 mm bars, all bar surfaces were ground using a 1200 grit diamond platen to remove surface damage to leave 2 mm × 2 mm × 4 mm final dimensions. Plastic deformation under compression at 1500 °C was studied in a mechanical frame (Zwick/Roll, Munich, Germany) equipped with a furnace with $MoSi_2$ heating elements. Plastic deformation under compression from 1800 °C to 2000 °C was studied in a mechanical frame (Instron, Norwood, USA) equipped with a furnace with tungsten heating elements (GT Technologies, New Hampshire, USA) operated at a pressure of approximately 9×10^{-3} Torr. Cross head speeds ranged from 5 μm/min to 100 μm/min. Push rods were protected by the use of SiC spacers, which are more creep resistant than materials tested in this work. Cross sections of specimens after compressive testing for scanning electron microscope (SEM) characterization were prepared using conventional methods involving successive steps of grinding and polishing with diamond slurries and cloths embedded with up to 1 μm diameter particles. The specimens were observed in an SEM equipped with a field emission gun (Hitachi S5200, Hitachi, Tokyo, Japan). Samples were examined in secondary electron (SE) imaging mode and backscattered electron (BS) image mode for atomic number contrast. Energy dispersive X-ray spectroscopy (EDS) was used to aid phase identification. Specimens for transmission electron microscopy (TEM), equipped with a LaB_6 gun (CM200, Philips, Eindhoven, Holland), were prepared using conventional methods of cutting, dimpling and ion milling. The TEM was equipped with an EDAX EDS detector (model R-TEM CM200, Mahwah, New Jersey, USA). Bright-field (BF) imaging and EDS were used to characterize the specimen microstructures and identify the different phases. Genesis spectrum TEM quantum materials software from EDAX was used to carry out the quantification of different elements during phase identification studies. Elemental C content analysis on powders found in HS20La after compressive deformation at 1800 °C were analysed by an elemental analyser (LECO CHNS 932, St. Joseph, Michigan, US).

The strain rate range studied was estimated, at a first approximation, as the thermal strain rate related to a heating rate in the range from 200 °C/min to 1000 °C/min, which could be a realistic heating rate range for hypersonic conditions, relating the thermal expansion to the thermal strain according to Eq. (2);

$$\dot{\varepsilon} = \alpha E \frac{\Delta T}{\Delta t} \tag{2}$$

where α is the coefficient of thermal expansion (CTE), E the elastic modulus and ΔT/Δt the heating rate. Heating rates of 200 °C/min and 1000 °C/min correspond to thermal strain rates of $2.8 \times 10^{-5}\,s^{-1}$ and $1.4 \times 10^{-4}\,s^{-1}$, respectively, at an elastic modulus of ~500 GPa [4] and CTE previously reported [6], which are in the range of interest for hypersonic applications.

3. Results and discussion

3.1. HS20 high temperature mechanical properties

Fig. 1 shows the creep response of HS20 from 1500 °C to 2000 °C approximately over the strain rate range $2.8 \times 10^{-5}\,s^{-1}$ and $1.4 \times 10^{-4}\,s^{-1}$ for strains as high as 24%. At 1500 °C (Fig. 1a), HS20 shows a limited ductility (< 6%) for strain rates $\dot{\varepsilon} < 6 \times 10^{-5}\,s^{-1}$. At higher strain rates, the deformation is increased to nearly 12% and significant softening is also observed. Deformation-induced softening could be related to either cavitation or phase instabilities. In addition, true steady states of deformation are only observed at 1900 °C or higher temperatures as softening is still active at 1800 °C. Stresses for the steady states of deformation were calculated through extrapolation of steady state to the initiation of the plastic regime at 1900 °C and 2000 °C, as plotted in Fig. 2a. Calculated stress exponents for the steady states of plastic deformation are shown in Fig. 2a, ranging from 3 to 1 as the temperature increases from 1500 °C to 2000 °C. In addition, calculated activation energies are 242 and 334 kJ/mol in the temperature ranges 1500–1800 °C and 1900–2000 °C respectively, suggesting the activation of different deformation mechanisms as the stress exponent also changes from 3 to 1 in these same temperature ranges. The last deformation state in Fig. 1c and 1d is not a true stationary as some softening is observed. Therefore, the stress exponent for this last deformation state might not be accurate and this state is not considered for the plot of stationary strain rates versus stress, so the stress exponent shown in Fig. 2a is more accurate than the one displayed for the last deformation state in Fig. 1c and 1d respectively. In addition, no true stationaries were observed at 1800C either, but the data points were considered to allow comparison with previously reported data. The satisfactory agreement of the calculated activation energy value with literature data in Fig. 2b suggests that it was a reasonable assumption.

Fig. 3 compares some of the previously reported data for the stationaries of plastic deformation on UHTCs. Studies at a strain rate below $10^{-5}\,s^{-1}$ [27–29] are not considered as they are out of the range of interest of hypersonic applications. HS20 is between 2 and 3 times more creep resistant than the ZS30 (ZrB_2 + 30 vol.% SiC) studied by Gangireddy et al. [22]. The different response could be attributed to the more refractory nature of HfB_2 compared to ZrB_2 or the lower SiC volume content of HS20 (20 vol.%) compared to ZS30 (30 vol.%). Talmy et al. studied the plastic response of ZrB_2 with SiC contents ranging from 0 to 50 vol.% and observed a change in the activation energy from 130 to 509 kJ/mol, showing a plastic behavior characterized by a lower SiC content giving a higher creep resistance. However, highly pure SiC is known to be extremely creep resistant and hard to sinter also, if no impurities or additives are present. Liquid phase sintering (usually from melting of silica contamination) or boron and carbon doping are common approaches in SiC to promote full densification [39–42] and avoid the use of temperatures of ~2200 °C required to sinter pure polycrystalline SiC by SPS [43]. For example, Fig. 2b reveals that additive-free nano β-SiC is 2–3 orders of magnitude more creep resistant at 1800 °C than HS20 at 1500 °C. In addition, liquid phase sintered SiC at 1756 °C is 1–2 orders of magnitude more creep resistant than HS20 at 1500 °C. Therefore, SiC is not playing any reinforcing role, or providing any improvement on the creep resistance, from a structural point of view which agrees with observations from Talmy et al. [27], who determined that the higher the SiC content, the higher the activation energy and the softer/lower the creep resistance. Fig. 2b shows activation energy versus SiC content calculated by Talmy et al. for ZrB_2 in which the activation data for this study are included. Note that Talmy et al.'s study is from 1200 to 1500 °C. Therefore, the activation energy used to make the comparison is the one obtained in this study in the lower temperature range studied (1500–1800 °C). Good agreement between our estimated activation energy and the activation energies of Talmy et al. [27] is shown in Fig. 2b, suggesting that SiC content might have a stronger influence on the plastic response of MeB_2 (Me = Zr, Hf) UHTCs than the kind of MeB_2 analyzed. This statement is supported by the plastic response of 1 wt.% boron-doped SiC in Fig. 2b at 1758 °C, which is similar to the plastic response of HS20 at 1800 °C, more creep resistant than ZS30 at 1800 °C, and shows a strong influence of B in the high temperature behavior of SiC. Liquid-phase sintered SiC and additive-free nano β-SiC are more than 3 orders of magnitude more creep resistant than 1 wt.% B-doped SiC at the same temperature (~1750 °C) [39,40,43], highlighting the enormous enhancement of creep rate or diffusion rate during plastic deformation by an addition of 1 wt.% B. There is a lack of data about plasticity of monolithic MeB_2 to confirm the role of SiC, but Melendez-Martinez et al. studied the plastic response under compressive creep of ZrB_2 from 1400 to 1600 °C [44]. In addition, it was reported that at 1500 °C ZrB_2 deforms at $\sim 10^{-7}\,s^{-1}$ under 400 MPa, which is ~300 times less resistant than HS20 reported herein in spite of ZrB_2 having a porosity of 13.5 vol.% [44]. Considering that there is little difference between the plastic response of ZS30 and HS20, as observed in Fig. 3, and also that the activation energy for ZrB_2 increases with the addition of SiC, it seems likely that the addition of

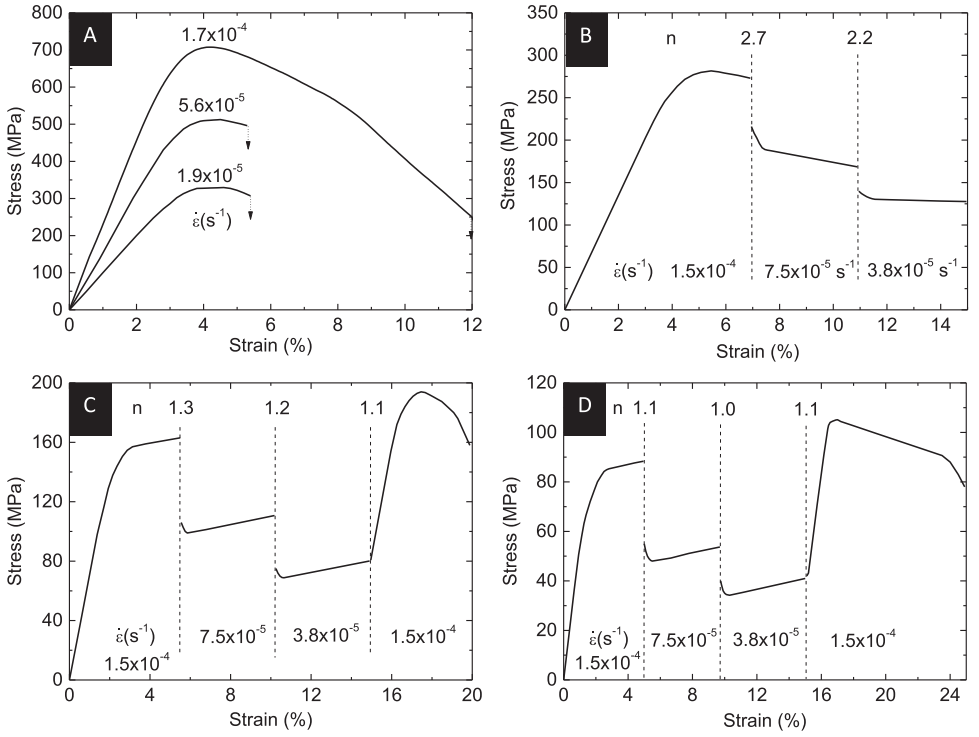

Fig. 1. Stress versus strain for HS20 at; a) 1500 °C, b) 1800 °C, c) 1900 °C and d) 2000 °C. Strain rates ($\dot{\varepsilon}$) for each deformation state and subsequent stress exponents (n) are shown.

SiC degrades the creep resistance of MeB_2 UHTCs. Furthermore, it indicates the need to characterize and understand the plasticity of MeB_2.

Concerning the high temperature creep properties of MeB_2 reinforced with MeC, there are a couple of studies in flexure for ZrB_2-20 vol.% ZrC and TiB_2-20 vol.% TiC in addition to other compositions with MeC contents in excess of 40 vol.%, which are far from the interest of this study [45,46]. ZrB_2 + 20 vol.% ZrC deforms at 2000 °C in the stress range 5–30 MPa with a strain rate range of 1.3-8.7 × 10^{-3} s^{-1} respectively and a stress exponent of n = 1, suggesting grain boundary sliding as the deformation mechanism. However, the ZrB_2-20 vol.% ZrC is nearly 100–150 times less creep resistant than the ZrB_2-20 vol.% ZrC studied by Gangireddy et al. [26] and HS20 from this study. In addition, contamination during milling of up to 6 wt.% with WC-Co was reported, which could explain the poor creep response of ZrB_2-20vol.% ZrC studied by Kats et al. [45] as Co melts at 1500 °C. This example illustrates how important it is to minimize contamination as undesired additional second phases can have a detrimental effect on physical properties at temperatures of 2000 °C or higher. Furthermore, monolithic ZrB_2 and TiB_2 were also studied at temperatures higher than 2000 °C [45,46]. However, if an extrapolation is made to 2000 °C, they are 100 times less creep resistant than ZS30 in the best case, which highlights the importance of controlling second phase impurities as well as the need to obtain reliable data on plasticity of monolithic MeB_2.

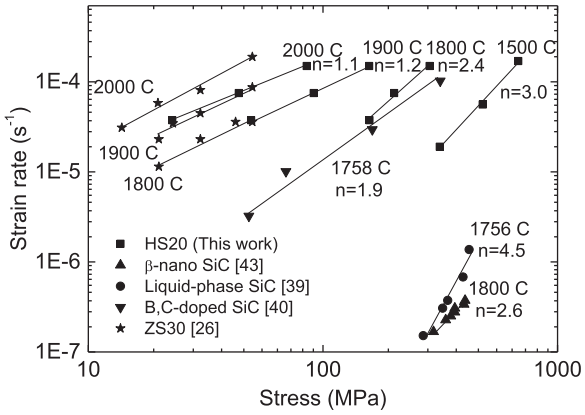

Fig. 3. Comparison of the strain rate versus stress from HS20 with previously reported data.

3.2. HS20 microstructural characterization after deformation

The concept of SiC-reinforced MeB_2 comes from the exceptional strength shown by SiC-ZrB_2 composites, as high as ~1 GPa [18], and the increased fracture toughness of MeB_2 with SiC additions, from

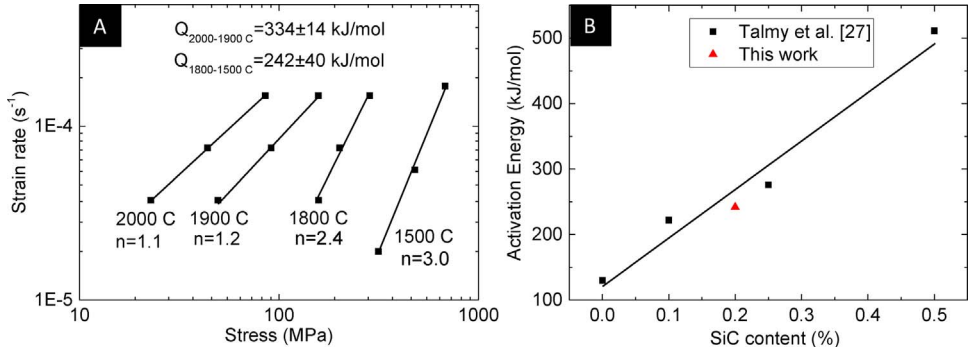

Fig. 2. a) Strain rate versus stress for the deformation stationary states of HS20. b) Comparison of the activation energy obtained in this study for the temperature range 1500–1800 °C with Talmy et. al study [27].

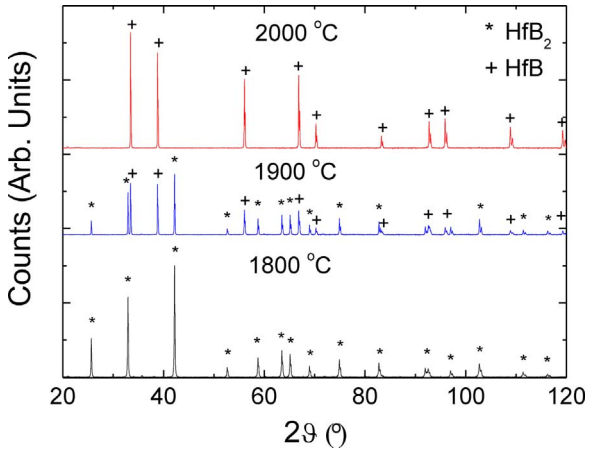

Fig. 4. XRD of the external surface of HS20 after deformation at 1800, 1900 and 2000 °C. XRD before deformation looks identical than after deformation at 1800 °C.

values of ~3 for monolithic MeB_2 to values as high as ~7 MPa/$m^{1/2}$ for composites with SiC [19]. However, this trend reverses at high temperature as SiC acts as a softening agent. A possible reason for this softening is the formation of an eutectic in the Me-B-C ternary system with a melting point of 2390 °C for Zr-B-C, which is nearly 1000 °C lower than the melting temperature of ZrB_2 [47]. In addition, the Me-B-C phase diagrams reported by Rudy and Windisch [48] suggestthat the combination of MeC + MeB_2 might be of interest at temperatures lower than 1500 °C as there could be temperature-dependent B-C exchange reactions associated with volume changes in the carbide particles, resulting in bodies with poor mechanical properties and subsequently limiting their high temperature potential use at temperatures above 1500 °C. If we consider the results observed here and previous available data [26,39,40,43], including the effect of 1 wt.% B in SiC, it could be concluded that B also has a negative effect on the high temperature mechanical behavior of MeB_2 + SiC systems. Fig. 4, shows XRD patterns of HS20 external surfaces before and after deformation revealing that at temperatures higher than 1800 °C, the formation of HfB is detected at the surface. However, XRD from an internal surface in the bulk does not show formation of HfB at any temperature. Plastic deformation is a phenomenon controlled by the bulk, so this observation could be considered as a confirmation of the existence of a B flux from the surface towards the bulk. Volatilization of B is unlikely as HfB_2 and B are stable in low vacuum atmospheres (~10^{-2} Torr).

Fig. 5 shows an SEM micrograph (top left) of the microstructure of HS20 after deformation at 2000 °C. In addition, different composition maps are shown as well as a line scan analysis. Moreover, B and Hf are detected in some areas from the original SiC secondary phase (dark contrast) in addition to Si and C being present in the HfB_2 matrix, which is also shown by the line analysis. A more in depth analysis by TEM reveals the formation of different phases as shown in Fig. 6. Different particles in the ternary Hf-Si-B system were detected by EDS after deformation at 2000 °C (Fig. 6a) and 1500 °C (Fig. 6b), suggesting bulk diffusion of B to produce a reaction forming new phases with different stoichiometries in the Hf-B-Si system. In addition, SiB_n particles were detected at 2000 °C (Fig. 6a). SiB_n particles with C-solid solubility and n as high as 32 have been observed previously [49]. Stoichiometry of phases determined by the semi-quantitative EDS used here is only approximate due to the difficulty of quantifying B by EDS. Some EDS spectra are shown in Fig. 7 as an example. After deformation at 1500 °C (Fig. 6b), 2 phases with brighter contrast in the Hf-Si-B-C and Hf-B-Si systems were detected by TEM. Dislocations are also present in the Hf-Si-B phase, in the magnified area indicated by an arrow, which is consistent with the observed stress exponent of 3 at 1500 °C. Cavitation damage, highlighted with circles in Fig. 6b, is also observed in samples deformed at 1500 °C, which could be responsible for the observed softening in the deformation curve. In addition, no signs of dislocations were observed at 1900 °C or 2000 °C consistent with either pure diffusional mechanisms or grain boundary sliding for micron-sized grains and measured stress exponents of 1 [36,37]. Talmy et al. [27] suggested grain boundary sliding as the deformation mechanism after studying the tensile side on 20 vol.%. SiC-reinforced ZrB_2 after flexure creep testing and observing the crack propagation. In addition, Bird et al. determined the activation of grain boundary sliding above 1600 °C, whereas pure diffusional mechanisms were active below 1600 °C [29]. The latter conclusion was supported by the observation of cavities being responsible for accommodating deformation. However, none of the previous studies carried out any detailed microstructural characterization by TEM. For example, cavities are observed in this study at 1500 °C, in which dislocations are observed (Fig. 6b) and a stress exponent of 3 is measured that is in agreement with a power law creep mechanism instead of grain boundary sliding. Typically, in ceramics with a grain size between 1 and 5 μm, a stress exponent between 2–1 is related to grain boundary sliding under compression [36,37]. However, this is true for ceramics without any phase evolution during

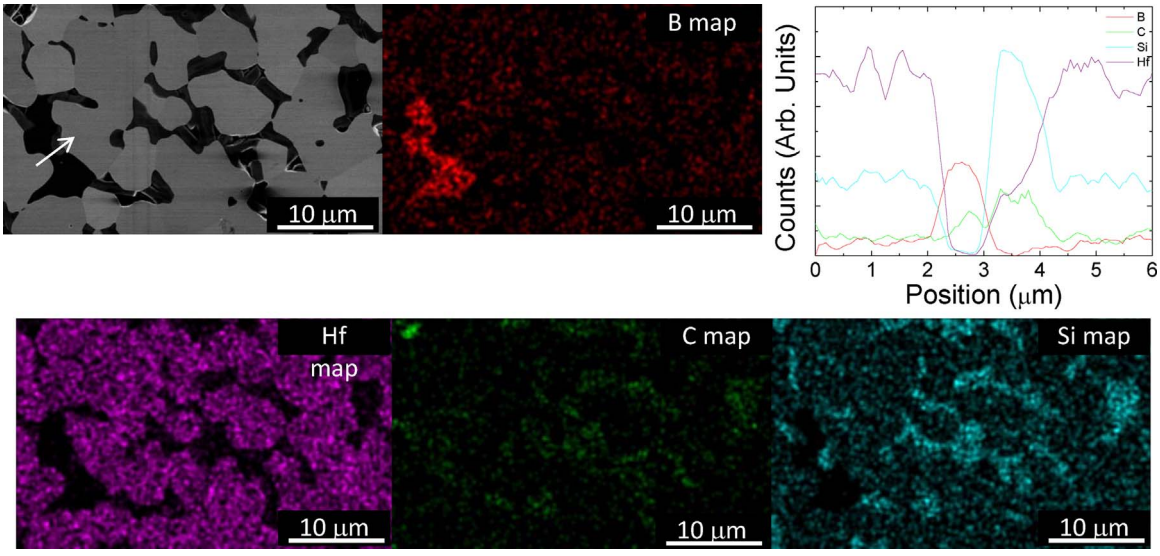

Fig. 5. SEM micrograph of HS20 after deformation at 2000 °C (top left) with the corresponding elemental mapping of B, Hf, C and Si. Also, a line analysis through the arrow in the micrograph is shown in the top right graph.

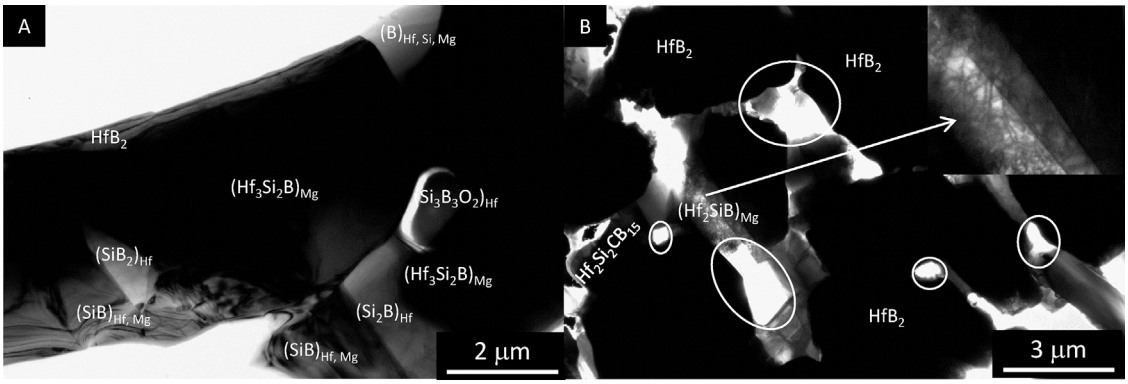

Fig. 6. a) BF TEM image of HS20 after deformation at 2000 °C. b) BF TEM image of HS20 after deformation at 1500 °C. Elements with concentrations below 5 at.% are considered as impurities and written as subscripts in the chemical formula.

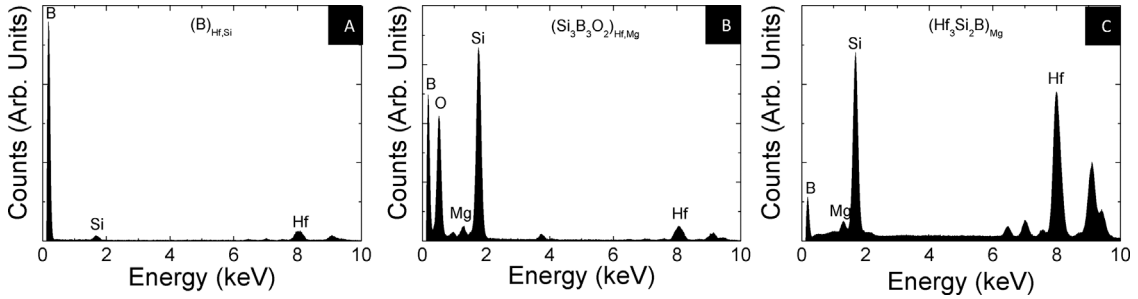

Fig. 7. EDS spectra of; a) $B_{Hf,Si}$, b) $(Si_3B_3O_2)_{Hf,Mg}$ and c) $(Hf_3Si_2B)_{Mg}$.

deformation, such as YTZP, Al_2O_3 or SiC among others [37]. Therefore, the possible activation of pure diffusional mechanisms in the temperature range 1900 °C–2000 °C cannot be ruled out due to phase evolution or formation of new phases in Hf-B-Si/Hf-B-Si-C systems during deformation. Furthermore, even in the case that grain boundary sliding is the active deformation mechanism, it requires the parallel activation of pure diffusional phenomena to produce the observed phase evolution.

In a recent study, Bird et al. confirmed the activation of grain boundary sliding during deformation of ZrB_2-20 vol.% SiC (ZS20) as indentation misalignments were observed after deformation as a consequence of grain boundary sliding, i.e. grain rotation and translation [31]. However, the activation energies reported were 364 and 639 kJ/mol for temperatures below 1600 °C or above 1600 °C [29], respectively, which are far higher than the ones reported by Talmy et al. [27], Gangirredy et al. [26] and this study, which are all in agreement. In fact, the creep rates reported by Bird et al. for ZS20 at 1800 °C are comparable to those reported for HS20 at 2000 °C in this study and similar to those reported for ZS30 at 1900 °C. This suggests that something is not being considered in Bird. et al. studies as their ZS20 should be more creep resistant than ZS30. It is noticeable in Fig. 15 of Bird et al. [29] that creep strain rate increases around 2 orders of magnitude from 1500 °C to 1550 °C under 100 MPa, while the difference in the creep strain rate at 100 MPa over all other temperatures shown is below an order of magnitude for a temperature difference of 100 °C. In addition, the experimental procedure shows that the powders were milled with WC-Co milling balls, which produced a WC-Co contamination of ~2.3 wt.% [29]. Co melting point is ~1500 °C highlighting how a relatively small amount of contamination can have a big impact on the high temperature creep response, which was not considered in the original study [29] or further microstructural characterization studies [31,50].

B diffusion through HfB_2 and SiC produces phase instabilities during plastic deformation at high temperature, as observed in this work, which is responsible for the lower creep resistance compared to pure SiC in Fig. 2b. Fig. 7 shows different phases with different stoichiometries observed and characterized by EDS, such as $B_{Hf,Si}$ (Fig. 7a), $(Si_3B_3O_2)_{Hf,Mg}$ (Fig. 7b) and $(Hf_3Si_2B)_{Mg}$ (Fig. 7c), in which the subscript elements are considered as impurities present as their content is below 5 at.%. A TPS material must be structurally stable with no phase instabilities. As a result we need to look for alternative UHTC systems from HS20. In addition, the fact that HfB is stable and could be formed according to the Hf-B phase diagram might explain the observed instabilities as some B could be released from HfB_2, diffusing to SiC particles [51] and leaving remnant HfB. ZrB_2-SiC ceramics might be more stable at such high temperatures since the Zr-B phase diagram does not show the formation of ZrB [48] as discussed previously by Portnoi and Romashov who concluded that if it forms it must be stabilized by the presence of some impurities, such as O or N [52]. Note that the equilibrium conditions of phase diagrams at high temperature do not correspond with our experimental conditions in the presence of stresses and subsequent deformation at high temperature. This might lead, for example, to effects such as reported by Seifert and Aldinger [53] who found SiC was stable in the presence of B_4C in the Si-B-C ternary system at 2500 K [48]. However, the presence of Hf is not addressed in their study [53] which could influence the stability of SiC in the Hf-Si-C-B quaternary system as Si diffuses towards HfB_2 (Fig. 5).

A comparison of HS20 microstructural evolution with ZrB_2-SiC UHTCs is not possible due to the lack of microstructural characterization of studies published to date carried out by TEM. Also, HfB exists in the binary Hf-B diagram while ZrB does not exist in the binary Zr-B diagram [48,51,52], which could result in different phase stabilities at high temperatures in Zr-Si-C-B and Hf-Si-C-B quaternary phase diagrams. For example, Gangireddy et al. [26] suggested symmetric plastic behavior according to the TEM study of Jayaseelan et al. [30], in which they did not observe any amorphous phase in the ZrB_2-SiC interphase. In our study, some borosilicate particles with minor Hf content were detected but only in samples which had been deformed at 2000 °C (Fig. 6), which suggests that the plastic response might not be symmetric, in agreement with Bird. et al. study [31]. Also, the plastic

response from a ZrB_2-30 vol.% SiC is similar to the HS20 studied here as there is only a factor of 2–3 difference in the strain rate for the steady states of the plastic deformation at the same stress level and same temperature. In addition, the fact that the activation energies agree well with those in the ZrB_2-SiC studied by Talmy et al. [27], suggests that similar mechanism to accommodate the deformation might be active (grain boundary diffusion). Neuman et al. [23] reported formation of liquid B-O-C-N inclusions in the only study including a TEM image after deformation from 1800 °C − 2300 °C, which are responsible for the strength degradation in this temperature range. However, microstructures after strength testing cannot be compared with those developed after compressive creep as the strength tests by Neuman et al. were measured under flexure and produced elastic failure, without there being time for diffusion to play a role in the microstructure development. Furthermore, an increase in the SiC cluster size was observed when testing at or above 1800 °C through *post mortem* SEM only [23]. Therefore, it is important that future studies give improved microstructural characterization to enable a better understanding of the phenomena involved in high temperature deformation.

Melendez-Martinez et al. [44] showed; (i) ZrB_2 at 1500 °C is 200 times more creep resistant than HS30 and (ii) the deformation mechanism is grain boundary sliding and that the deformation of individual ZrB_2 grains could be neglected as well as any contribution to deformation from ZrB_2-ZrB_2 grain boundaries. Therefore, grain boundaries of secondary phases with ZrB_2 and with the secondary phases are responsible for the macroscopic deformation and link the B diffusion to form new secondary phases in the Hf-B-Si and Hf-B-Si-C systems as the existing accommodation process of the deformation mechanism. However, it is difficult to assess how the formation of these secondary phases start and how each phase contributes to macroscopic deformation. Future studies at low deformations will try to answer how instabilities are triggered and how deformation is controlled in the initial stage of plastic deformation. In summary, our study suggests that HS20 behaves at high temperature as follows; (i) a power law creep with thermal activation process accommodated by B lattice diffusion ($n = 3$ and $Q = 242$ kJ/mol) in the temperature range 1500–1800 °C, consistent with the observation of dislocations by TEM, (ii) grain boundary sliding/pure diffusional mechanism accommodated by B grain boundary diffusion ($n = 1$ and $Q = 334$ kJ/mol), consistent with the absence of dislocations and the generation of new phases in the Hf-B-Si and Hf-B-Si-C systems.

3.3. HS20La high temperature mechanical properties

2 wt.% addition of La to HS20 (HS20La) helps reduce the internal stresses produced during cooling in the SPS without altering mechanical properties at RT, such as strength and toughness [19]. In addition, La addition stabilizes the thermal conductivity in the temperature range from 1500 °C to 1900 °C due to a compensation of CTE mismatch between SiC and HfB_2 as La_2O_3 is located next to SiC particles [6], which could be an advantage for designers when calculating UHTCs performance [3]. Moreover, La_2O_3 addition stabilizes the long-term response during oxidation at 1500 and 1600 °C due to the formation of Hf-O-C particles which slow down growth of the oxide protective layer [11]. Therefore, unlike HS20 HS20La could be a good candidate for hypersonic applications. However, Fig. 8 reveals that the plastic response is far from being satisfactory for several reasons; (i) There is a sudden softening after the end of elastic deformation suggesting development of structural damage with the plastic deformation, (ii) the lack of a true deformation stationary as softening is observed under any of the conditions studied, and (iii) HS20La is even less creep resistant than HS20 (Fig. 8b). There was no attempt to calculate activation energies as no true stationary state was observed under any condition. In addition, the stress exponents given in Fig. 8 are only indicative to enable a quick comparison with HS20 but they were not calculated with the intention of suggesting a deformation mechanism.

La_2O_3 addition does not act as a high temperature structural reinforcement. In addition, powders were observed immediately around the sample after testing at 1800 °C, a smaller amount (< 10 mg) of powder was observed at 1900 °C but no trace of powder was observed at 2000 °C, which could be related to the development of either porosity next to the external surface or a chemical reaction during deformation. C content of the powders found at 1800 °C was 1.70 ± 0.02 wt.%. However, the amounts of powder collected at 1900 °C were not enough for C content analysis. Considering that C content for HS20La is 2.01 wt.%, the latter finding suggests that SiC might segregate in Si and free C at 1800 °C. Moreover, the higher the temperature, the lower the porosity detected at the external surface as diffusion phenomena are more active balancing the presence of any damaging mechanisms such as cavitation or reaction (Fig. 9). For example, Fig. 9a shows the cross section after compression testing at 1800 °C, in which the highest degree of porosity is observed and is reduced as temperature increases to 1900 °C (Fig. 9b) and 2000 °C (Fig. 9c). In a previous study, La_2O_3 particles were observed to be located next to SiC particles [19] which could have an influence on the SiC disociation as this phenomena was not observed in HS20. However, after deformation at 2000 °C there was no O in what were originally La_2O_3 particles as shown in Fig. 10. The remnant La_2O_3 particle contains La-Si-Hf-B after deformation, which suggests that O might react with C from SiC particles. Also, the stoichiometry of the SiB_n particles is different in HS20 than HS20La: the maximum n in HS20 is 2 whereas it is 12 for HS20La. In addition, SiB_n particles with $n > 2$ contain minor amounts of La, indicating that La plays a role in the formation of new SiB_n phases during deformation, which are not formed otherwise. SiB_n as a solid solution with n as high as 32 has been reported [49]. Also, some of the SiB_n decomposes through a peritectic reaction involving liquid formation, e.g. SiB_6 (observed in Fig. 10), which decomposes to a liquid plus SiB_n with $n > 6$. The decomposition temperature of SiB_6 is 1850 °C but how Hf and La could affect the stability of SiB_6 is unknown. Our study indicates that if decomposition reaction occurs, it has to be above 1900 °C as a stress exponent of 3 could be a clear indication of dissolution-precipitation deformation mechanism in ceramics where a liquid is present at the grain boundaries. This is also indicated by the presence of rounded grains in Fig. 10 on SiB_n particles with $n > 6$. Disociation/Decomposition of SiC or SiB_n phase could be responsible for the mechanical resistance degradation observed in the stress-deformation curves (Fig. 8). However, to clarify which phase is responsible for the mechanical response degradation, the initial stage of deformation should be studied in detail, which is beyond the scope of this work and will be the subject of future studies. Nonetheless, the poor creep resistance shown by HS20La highlights an unsatisfactory behavior for hypersonic re-entry involving temperatures in excess of 1800 °C. Besides, the use of RE-oxides or any oxide is not recommended according to these results in spite of having the ability to either develop dense-oxidation-resistant RE-zirconates/hafnates layers or stabilize oxidation formation through the presence of Zr-O-C/Hf-O-C particles.

Assuming the conditions of temperature and stresses described above, 1800 °C and 400 MPa, and the results from this study (Fig. 8), we suggest (i) HS20 is deforming at $3 \times 10^{-4}\,s^{-1}$ and (ii) HS20La at $10^{-3}\,s^{-1}$. In addition, plastic deformation at 1800 °C starts at around 4% and 3% for HS20 and HS20La (Fig. 1 and 8), so that at stresses below 400 MPa there will be no dimension changes for 130 s and 30 s respectively. Moreover, 10% deformation will be reached in 330 s and 100 s respectively. In a sharp leading edge component the deformation should not go above 10% under any circumstances due to the negative impact on flight aerodynamics. Therefore, considering that an atmospheric re-entry lasts around 10 min being at least half of the time under the hardest conditions, i.e. 1800C and 400 MPa in this discussion, only HS20 would be able to withstand it with a deformation below 10% (9% approximately) while HS20La would be far above 20% deformation, mechanically failing before the end of the re-entry. Ideally, the material should not exceed elastic deformation to be reusable from

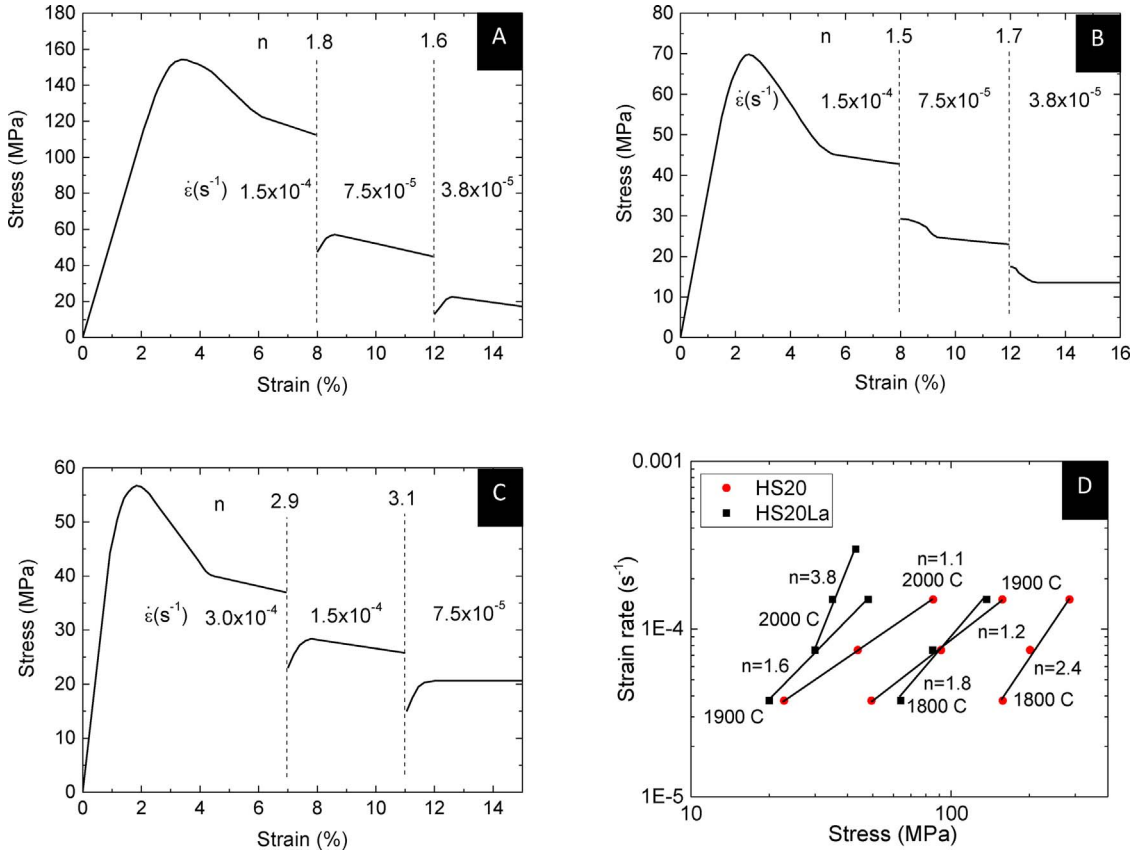

Fig. 8. Stress versus strain for HS20La at; a) 1800 °C, b) 1900 °C and c) 2000 °C. Strain rates for each deformation state are shown. d) Strain rate versus stress for the deformation stationaries of HS20 and HS20La.

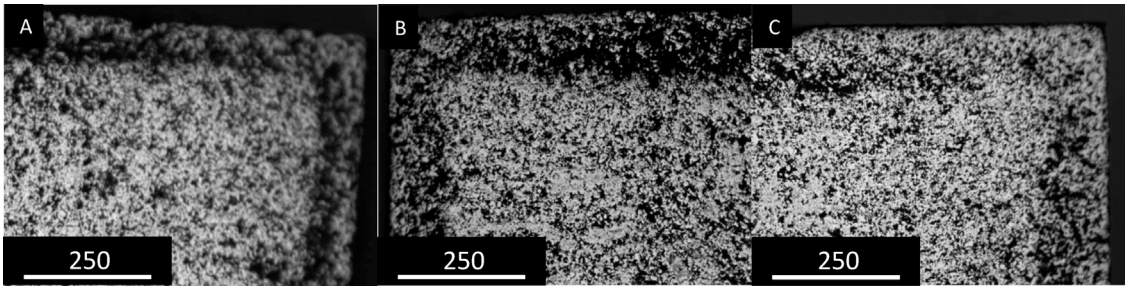

Fig. 9. Cross section image of HS20La after deformation at; a) 1800 °C, b) 1900 °C and c) 2000 °C.

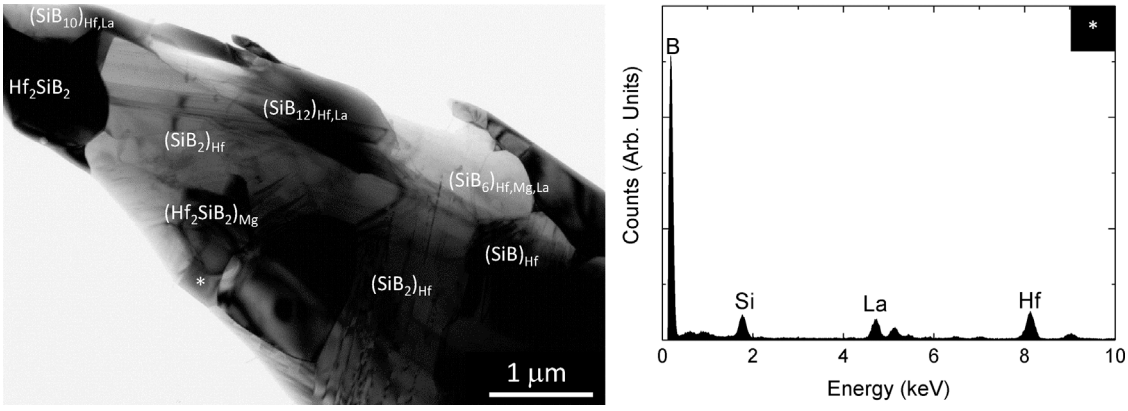

Fig. 10. BF TEM picture of HS20La after deformation at 2000 °C with an EDS spectra for the phase with a *.

a structural point of view although those materials exceeding the elastic deformation developing a certain shape change such as HS20 might be suitable for single use. Considering other UHTCs studied, ZrB_2-30 vol.% SiC deforms at $5 \times 10^{-4}\,s^{-1}$, which means that it is slightly out of the secure range defined in this study as a 10% deformation and the elastic threshold (4%) will be reached in 200 s and 80s, respectively. ZrB_2-20 vol.% SiC samples tested under plasma wind tunneling testing conditions showed the tip of a sharp leading edge was slightly curved and deformed afterwards even if testing times were no longer than 50 s [54]. Note that 1800 °C and 400 MPa are mild re-entry conditions and ideally materials capable of withstanding re-entries with temperatures in excess of 2000 °C are needed in the long term. For example, none of the MeB_2-based UHTCs analyzed in either this study or previous studies could survive without deforming less than 10% at 2000 °C under 200 MPa, which highlights a need for new UHTCs and approaches. In addition, there is a lack of studies about deformation mechanisms in the UHTCs community in the temperature range 1800–2000 °C and in the strain range rate of interest (10^{-5}-$10^{-4}\,s^{-1}$). Therefore, it is difficult to make an assessment about structural performance of UHTCs under realistic mechanical stresses at temperatures of interest. Nonetheless, the data reported till now indicate that alternatives should be explored. Furthermore, the creep resistance of MeB_2 UHTCs is completely unknown and it should be studied before the UHTCs community can understand how these materials might be structurally reinforced.

4. Conclusions

High temperature compressive creep of HS20 and HS20La UHTCs up to 2000 °C reveals that HS20 might withstand the proposed conditions for a single use in hypersonic reentries but materials with higher creep resistance should be developed. RE oxide additions to HS20 degraded the creep resistance compared to HS20. Therefore, it is necessary to explore other systems as well as understanding the creep response of monolithic materials to indicate how they could be structurally reinforced.

Acknowledgments

The Authors' acknowledge Prof. Mike Reece, Nanoforce Technology Ltd., Queen Mary, University of London, UK for providing access to the Spark Plasma Sintering facility. EZS also acknowledges support through a contract from the JAE-DOC program of CSIC, Spain, co-funded by the FSE to carry out this research project (2012–2015). DGG, ADR and EZS acknowledge the project MAT2015-71411-R from MINECO (Spain). EZS and WEL acknowledges the EPSRC grant XMAT (EP/K008749/1) for supporting this research and EZS while doing compression testing at Imperial College London.

References

[1] A.E. McHale, Phase Equilibria Diagrams for Ceramists: Borides, Carbides and Nitrides, American Ceramic Society, Westerville, 1994.
[2] A. Paul, D.D. Jayaseelan, S. Venugopal, E. Zapata-Solvas, J. Binner, B. Vaidhyanathan, A. Heaton, W.E. Lee, UHTC composites for hypersonic applications, Bull. Am. Ceram. Soc. 91 (2011) 22.
[3] T.H. Squire, J. Marschall, Material property requirements for analysis and design of UHTC components in hypersonic applications, J. Eur. Ceram. Soc. 30 (2010) 2239.
[4] W.G. Fahrenholtz, G.E. Hilmas, I.G. Talmy, J.A. Zaykoski, Refractory diborides of zirconium of hafnium, J. Am. Ceram. Soc. 90 (2007) 1347.
[5] M.M. Opeka, I.G. Talmy, E.J. Wuchina, J.A. Zaykoski, S.J. Causey, Mechanical, thermal, and oxidation properties of refractory hafnium and zirconium compounds, J. Eur. Ceram. Soc. 19 (1999) 2405.
[6] E. Zapata-Solvas, D.D. Jayaseelan, P. Brown, W.E. Lee, Thermal properties of La_2O_3-doped ZrB_2- and HfB_2-based ultra-high temperature ceramics, J. Eur. Ceram. Soc. 33 (2013) 33.
[7] D. Sciti, A. Balbo, A. Bellosi, Oxidation behavior of a pressureless sintered HfB_2-$MoSi_2$ composite, J. Eur. Ceram. Soc. 29 (2009) 1809.
[8] E. Opila, S. Levine, J. Lorincz, Oxidation of ZrB_2- and HfB_2-based ultra-high temperature ceramics: effect of Ta additions, J. Mater. Sci. 39 (2004) 5969.
[9] E. Eakins, D.D. Jayaseelan, W.E. Lee, Toward oxidation-resistant ZrB_2-SiC ultra high temperature ceramics, Metall. Mater. Trans. A 42 (2011) 878.
[10] D.D. Jayaseelan, E. Zapata-Solvas, P. Brown, W.E. Lee, *In situ* formation of oxidation resistant refractory coatings on SiC-reinforced ZrB_2 ultra high temperature ceramics, J. Am. Ceram. Soc. 95 (2012) 1247.
[11] E. Zapata-Solvas, D.D. Jayaseelan, P.M. Brown, W.E. Lee, Effect of La_2O_3 addition on long-term oxidation kinetics of ZrB_2-SiC and HfB_2-SiC ultra-high temperature ceramics, J. Eur. Ceram. Soc. 34 (2014) 3535.
[12] C.M. Carney, Oxidation resistance of hafnium diboride-silicon carbide from 1400 °C to 2000 °C, J. Mater. Sci. 44 (2009) 5673.
[13] C.M. Carney, T.A. Pathasarathy, M.K. Cinibulk, Oxidation resistance of hafnium diboride ceramics with additions of silicon carbide and tungsten boride or tungsten carbide, J. Am. Ceram. Soc. 94 (2011) 2600.
[14] P. Hu, W. Guolin, Z. Wang, Oxidation mechanism and resistance of ZrB_2-SiC composites, Cor. Sci. 51 (2009) 2724.
[15] W.B. Han, P. Hu, X.H. Zhang, J.C. Han, S.H. Meng, High-temperature oxidationat 1900 °C of ZrB_2-xSiC ultrahigh-temperature ceramic composites, J. Am. Ceram. Soc. 91 (2008) 3328.
[16] M. Tului, S. Lionetti, G. Pulci, E. Rocca, T. Valente, G. Marino, Effects of heat treatments on oxidation resistance and mechanical properties of ultra high temperature ceramic coatings, Surf. Coat. 202 (2008) 4394.
[17] P. Hu, X.H. Zhang, J.C. Han, X.G. Luo, S.Y. Du, Effect of various additives on the oxidation behavior of ZrB_2-based ultra-high-temperature ceramics at 1800 °C, J. Am. Ceram. Soc. 92 (2010) 345.
[18] A.L. Chamberlain, W.G. Fahrenholtz, G.E. Hilmas, High-strength zirconium diboride-based ceramics, J. Am. Ceram. Soc. 87 (2004) 1170.
[19] E. Zapata-Solvas, D.D. Jayaseelan, P.M. Brown, W.E. Lee, Mechanical properties of ZrB_2- and HfB_2-based ultra-high temperature ceramics fabricated by spark plasma sintering, J. Eur. Ceram. Soc. 33 (2013) 1373.
[20] S. Zhu, W.G. Fahrenholtz, G.E. Hilmas, Influence of silicon carbide particle size on the microstructure and mechanical properties of zirconium diboride-silicon carbide ceramics, J. Eur. Ceram. Soc. 27 (2007) 2077.
[21] E.W. Neuman, G.E. Hilmas, W.G. Fahrenholtz, Strength of zirconium diboride to 2300 °C, J. Am. Ceram. Soc. 96 (2013) 47.
[22] P. Hu, Z. Wang, Flexural strength and fracture behavior of ZrB_2-SiC ultra-high temperature ceramics composites at 1800 °C, J. Eur. Ceram. Soc. 30 (2010) 1021.
[23] E.W. Neuman, G.E. Hilmas, W.G. Fahrenholtz, Mechanical behavior of zirconium diboride-silicon carbide-boron carbide ceramics up to 2200 °C, J. Am. Ceram. Soc. 35 (2016) 463.
[24] E.W. Neuman, G.E. Hilmas, W.G. Fahrenholtz, Ultra-high temperature mechanical properties of a zirconium diboride-zirconium carbide ceramic, J. Am. Ceram. Soc. 99 (2016) 597.
[25] E.W. Neuman, G.E. Hilmas, W.G. Fahrenholtz, Mechanical behavior of zirconium diboride-silicon carbide ceramics at elevated temperature in air, J. Am. Ceram. Soc. 33 (2013) 2889.
[26] S. Gangireddy, J.W. Halloran, W.N. Zachary, Flexural creep of zirconium diboride-silicon carbide upto 2200 °C in minutes with non-contact electromagnetic testing, J. Eur. Ceram. Soc. 33 (2013) 2901.
[27] I.G. Talmy, J.A. Zaykoski, C.A. Martin, Flexural creep deformation of ZrB_2/SiC ceramics in oxidizing atmosphere, J. Am. Ceram. Soc. 91 (2008) 1441.
[28] W.M. Guo, G.J. Zhang, H.T. Lin, High temperature flexural creep of ZrB_2-SiC ceramics in argon atmosphere, Ceram. Int. 38 (2012).
[29] M.W. Bird, R.P. Aune, F. Yu, P.F. Becher, K.W. White, Creep behavior of a zirconium diboride-silicon carbide composite, J. Eur. Ceram. Soc. 33 (2013) 2407.
[30] D.D. Jayaseelan, Y. Wang, G.E. Hilmas, W.G. Fahrenholtz, P. Brown, W.E. Lee, TEM investigation of hot pressed −10 vol% SiC-ZrB_2 composite, Adv. Appl. Ceram. 110 (2011) 1.
[31] M.W. Bird, P.F. Becher, K.W. White, Grain rotation and translation contribute substantially to creep of a zirconium diboride silicon carbide composite, Acta Mater. 89 (2015) 73.
[32] R. Riedel, I.W. Chen, Ceramics Science and Technology, Vol. 2 Materials and Properties, Wiley-VCH, Weinheim, 2010.
[33] K.J. Yoon, S.M. Wiederhorn, W.E. Luecke, Comparison of tensile and creep behavior in silicon nitride, J. Am. Ceram. Soc. 83 (2000) 2017.
[34] S.M. Wiederhorn, B.J. Hockey, J.D. French, Mechanisms of deformation of silicon nitride and silicon carbide at high temperatures, J. Eur. Ceram. Soc. 2273 (1999) 2273.
[35] A. Bravo, M. Jimenez, A. Dominguez, A.H. Chokshi, The role of a threshold stress in the superplastic deformation of fine-grained yttria-stabilized zirconia polycrystals, Scr. Metall. Mater. 34 (1996) 1155.
[36] E. Zapata-Solvas, D. Gomez-Garcia, C. Garcia-Gañan, A. Dominguez-Rodriguez, High temperature creep behavior of 4 mol% yttria tetragonal zirconia policristals (4-YTZP) with grain sizes between 0.38 and 1.15 μm, J. Eur. Ceram. Soc. 27 (2007) 3325.
[37] D. Gomez-Garcia, E. Zapata-Solvas, A. Dominguez-Rodriguez, L.P. Kubin, Diffusion-driven superplasticity in ceramics: modeling and comparison with available data, Phys. Rev. B 80 (2009) 214107.
[38] E. Zapata-Solvas, D.D. Jayaseelan, P. Brown, W.E. Lee, Effect of oxidation on room temperature strength of ZrB_2- and HfB_2-based ultra-high temperature ceramics, Adv. Appl. Cer. 114 (2015) 407.
[39] M. Castillo-Rodriguez, A. Munoz, A. Dominguez-Rodriguez, Correlation between microstructure and creep behaviour in liquid-phase-sintered α-Silicon Carbide, J. Am. Ceram. Soc. 89 (2006) 960.
[40] Y. Shinoda, M. Yoshida, T. Akatsu, F. Wakai, Compression deformation mechanism of silicon carbide: I, fine-grained boron- and carbon-doped β-Silicon carbide fabricated by hot isostatic pressing, J. Am. Ceram. Soc. 87 (2004) 1919.
[41] A.L. Ortiz, A. Muñoz, O. Borrero, A. Domínguez, F. Guiberteau, N.P. Padture, Effect

of sintering atmosphere on the mechanical properties of liquid-phase sintered SiC, J. Eur. Ceram. Soc. 24 (2004) 3245.
[42] M. Castillo, A. Muñoz, A. Domínguez-Rodriguez, Effect of atmosphere and sintering time on the microstructure and mechanical properties at high temperatures of α-SiC sintered with liquid phase Y_2O_3-Al_2O_3, J. Eur. Ceram. Soc. 26 (2006) 2389.
[43] A. Lara, A. Munoz, M. Castillo-Rodriguez, A. Dominguez-Rodriguez, High-temperature compressive creep of spark-plasma sintered additive-free polycrystalline β-SiC, J. Eur. Ceram. Soc. 32 (2012) 3445.
[44] J.J. Melendez-Martinez, A. Dominguez-Rodriguez, F. Monteverde, C. Melandri, G. de Portu, Characterisation and high temperatura mechanical properties of zirconium boride-based materials, J. Eur. Ceram. Soc. 22 (2002) 2543.
[45] S.M. Kats, S.S. Ordan'yan, V.I. Unrod, Compressive creep of alloys of the ZrC-ZrB_2 and TiC-TiB_2 systems, Poroshkvaya Metallurgiya 12 (228) (1981) 70.
[46] I.I. Spivak, R.A. Andrievskii, V.V. Klimenko, V.D. Lazarenko, Creep in the binary systems TiB_2-TiC and ZrB_2-ZrN, Poroshkvaya Metallurgiya 8 (140) (1973) 17.
[47] E.W. Neuman, H.J. Brown-Shaklee, J. Watts, G.E. Hilmas, W.G. Fahrenholtz, Case study: building an ultra-high temperature mechanical testing system, Bull. Am. Ceram. Soc. 92 (2012) 36.
[48] E. Rudy, S. Windisch, Ternary Phase Equilibria in Transition Metal-Boron-Carbon-Silicon Systems, AFML, Ohio, 1966.
[49] J. Roger, V. Babizhetskyy, J.F. Halet, R. Guerin, Boron-silicon solution: synthesis and crystal structure of a carbon-doped boron-rich SiB (n ~ 30) compound, J. Solid State Chem. 177 (2004) 4167.
[50] C.H. Yu, M.W. Bird, C.W. Huang, C.S. Chen, Y.F. Gao, K.W. White, C.H. Hsueh, Micromechanics modeling of creep fracture of zirconium diboride-silicon carbide composites at 1400-1700 °C, J. Eur. Ceram. Soc. 34 (2014) 4145.
[51] P. Rogl, P.E. Potter, A critical review and thermodynamic calculation of the binary system: hafnium-boron, CALPHAD 12 (1988) 207.
[52] K.I. Portnoi, V.M. Romashov, Binary constitution diagrams of systems composed of various elements and boron–a review, Poroshkovaya Metallurgiya 5 (1972) 48.
[53] H.J. Seifert, F. Aldinger, Structure and Bonding Phase Equilibria in the Si-C-B-N System. Vol 101 in Structure & Bonding, Springer-Verlag, Berlin, 2002.
[54] F. Monteverde, R. Savino, ZrB_2-SiC sharp leading edges in high enthalpy supersonic flows, J. Am. Ceram. Soc. 95 (2012) 2282.